UNIVERSITÀ DEGLI STUDI DI BERGAMO

Facoltà di Ingegneria

Corso di Laurea Specialistica in Ingegneria Meccanica

Classe n. 36/S – ingegneria meccanica

Computational solution of fluid-structure interaction in human carotids: A comparison before and after the plaque removal

Relatore:

Chiar.mo Prof. Christian Vergara

Correlatore:

Dott. Matteo Pozzoli

Tesi di Laurea Specialistica

Paolo Ghilardi

Matricola n. 49364

ANNO ACCADEMICO 2011 / 2012

Contents

1 Introduction to computational haemodynamics **5**

2 Mathematical description of the problem **9**
2.1 Fluids equations 9
2.1.1 Navier-Stokes equations 10
2.1.2 Arbitrarian Lagrangian Eulerian formulation of Navier-Stokes equations 12
2.2 Finite elasticity equations 14
2.3 Coupled Fluid-Structure interaction (FSI) problem 16

3 Numerical discretization **19**
3.1 A brief introduction to the FEM 19
3.1.1 Weak formulation of the Poisson's problem 21
3.1.2 The Galerkin's problem 22
3.1.3 Solution of the Poisson's problem with FEM 23
3.2 Discretization of the problem in time 24
3.3 Partioned Algorithms for the Numerical Solution 26
3.3.1 The double-loop iteration scheme 27

4 A clinical application **31**
4.1 Introduction to Atherosclerosis 31
4.2 Setting of the boundary conditions and sensitivity of the numerical solution respect to the mesh 34
4.3 Comparison before and after the removal of the plaque 37
4.3.1 Mean pressure and flux 38
4.3.2 Velocity 40
4.3.3 Wall displacement 42
4.3.4 Wall shear stress (WSS) 43
4.4 Final comment on the results obtained 45

Bibliography **47**

Chapter 1

Introduction to computational haemodynamics

The cardiovascular system has the task of supplying the human organs with oxigen and nutrients. Its main components are the heart, the arteries and the veins. The large (systemic) circulation brings oxygenated blood from the left ventricle via the aorta to the various organs through the arterial system, then brings it back through the venous system and the vena cava to the right atrium. The small circulation connects the heart and the lungs. Blood is pumped from the right ventricle via the pulmonary artery to the lungs, then via the pulmonary vein oxigenated blood returns to the heart, where is pumped to all organs.[3]

The fundamental importance of cardiovascular system in life led some of the greatest scientist of all time as Aristoteles, Euler, Bernoulli to its study. In modern times the great social impacts of cardiovascular diseases, responsible today of about 40 % of deaths in developed countries, gave further motivation to study in deep how heart and blood vessel's work[3]. Until Seventies the only way to study cardiovascular system were experiments on animals and *in vitro*. Later, thanks to the great improvement in computing power, suitable algoritms have been developed such that, starting from realistic geometries and clinical data obtained from exams as magnetic resonance, digital angiography, Doppler anemometry [6], they can simulate blood flow. In this way can be valued data that can not be obtained from laboratory experiments, like shear stress on vessel's wall, and so improve the knowledge of circulatory system.[3]

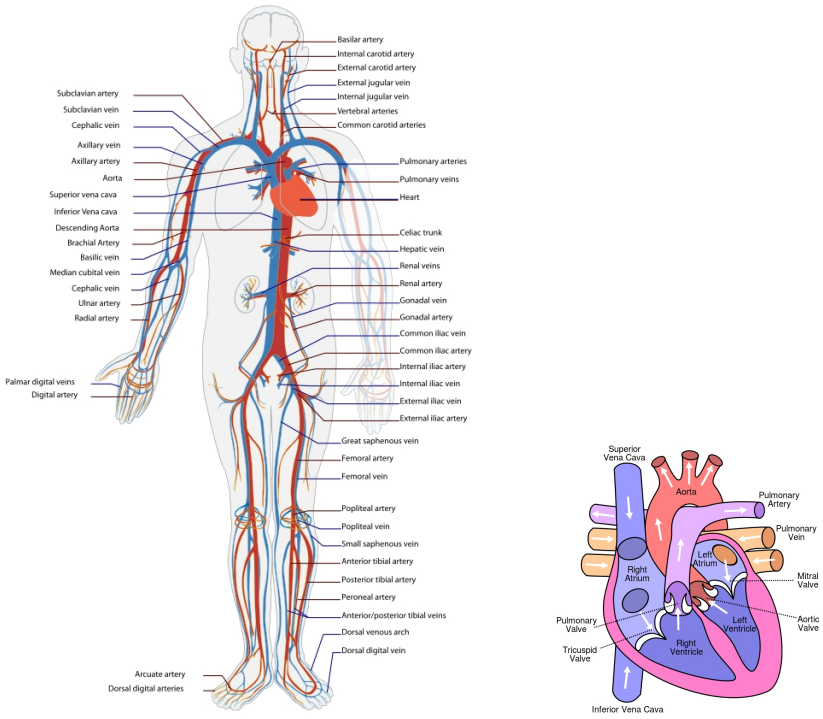

Figure 1.1: A representation of the main blood vessels and of the heart

Simulation of blood flow involves some mathematical difficulties. The first, and perhaps more relevant, is the unsteadiness of blood flow. The arterial pulsatility induced by the the heart action strongly influences haemodynamics [21]. Fast transients are therefore a relevant feature of blood flow and specific numerical techniques for their reliable simulations are required, particularly when one is interested in blood flow in large arteries (those whose diameter is above 0.4mm)[18].

Another serious difficulty is that haemodynamics includes different phenomena interacting among them. At the mathematical level, this implies the coupling of different models acting either in the same computational domain or in adjacent subdomains and related by appropriate interface or matching conditions [1]. Their numerical treatment then require the formulation of appropriate algorithms to treat these coupling conditions[18].

A further important feature of haemodynamic problems is the presence of multiple scales in both time and space. An illustrative instance is represented by the regulation of blood flow distribution. A stenosis (i.e a significant lumen reduction) in an artery does not necessarily cause a relevant reduction of blood supply to the downstream compartments. Indeed blood may be redistributed through other vessels and continue to ensure an almost physiological

value of blood flow. These changes are activated by biochemical mechanisms which govern vessel dilatation and may even drive the oxygen exchange between blood and tissues. Here, we face different time scales (blood flow and regulation mechanisms) and spatial scales (the local heamodynamics and the global circulatory system)[18].

Computational haemodynamics can be helpful not only to study and better understand the blood dynamics in a given vascular district or but also for solve inverse problems, for example determine the optimal shape of a prosthetic implant to guarantee certain values of blood flow in a organ. The major difficulty in solving inverse problems in general is represented by the severe computational costs. Optimization solvers are usually based on iterative procedures and this could be prohibitely expensive if each iteration requires the solution of a system of non-linear time-dependent partial differential equations. For this reason, specific techniques are under development, aiming at reducing the computational costs[18].

In this thesis work is exposed the problem of the simulation of an artery using the Finite Elements Method. The object of study was the left carotids, the intent was to obtain information of how important parameters of the blood flow and the vessel's wall change in presence of a atherosclerotic plaque at the bifurcation of the common carotid. From the mathematical point of view this problem involves some of the mathematical difficulties exposed above, in particular the problem to have a fluid and a structure that undergoes large deformations interacting between them (fluid structure interaction, or FSI, problem). A possible mathematical model that traeats this problem will be exposed in chapter two, then in chapter three will be explained the numerical techniques used to solve the problem and finally in chapter four will be showed the results obtained from the simulations .

Chapter 2

Mathematical description of the problem

In this chapter the mathematical model used to descibe blood flow in human carotids will be presented. In section 2.1 the reology model chosed to represent blood will be showed and also how the problem of describe a fluid that flow in a moving domain have been solved. In section 2.2 the equations and the constituive law used to model vessel's wall will be exposed. In section 2.3 how the two problems are coupled will be explained.

2.1 Fluids equations

Blood is a solution of different tipe of particles (such as red blood cells, white blood cells, platelets) in an aqueous solution called plasma.

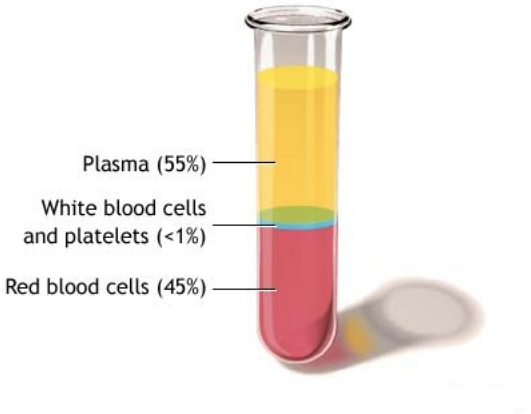

Figure 2.1: **Blood Composition**. Percentuals of main components are reported

Blood in general is charcterized by a non constant density and features a compressible behaviour. However, considering large vessel (diameter>0.1 cm), as carotids are, we can assume it is homogeneous and incompressible [15]. Moreover, in such districts, it can be assumed to be Newtonian, that is the relation between stress and strain is assumed to be linear. Therefore we can model blood using *Navier-Stokes* equations. Another important thing is that is not necessary to indroduce a turbulence model because blood flow, most often, it is laminar. In normal physiological situations, the values of the Reynolds number [1] reached in the cardiovascular system do not allow the formation of full scale turbulence[18], as it can be seen in the following table.

Vessel	Diameter [cm]	Velocity [cm/s]	Reynold's Number
Aorta	2.5	48	3400
Arteries	0.4	45	500
Arterioles	0.005	5	0.7
Capillaries	0.0008	0.1	0.002
Venules	0.002	0.2	0.01
Veins	0.5	10	140
Vena Cava	3	38	3300

Table 2.1: Blood vessels types and their main characteristics

Fluid equations will be written using *Arbitrarian Lagrangian Eulerian formulation*. Is necessary use this formulation because the fluid domain boundary is composed by a physical boundary (the vessel's wall) that is moving and artificial boundaries (the inlet and outlet sections) that must remain fixed during the time interval in which the problem will be solved.

2.1.1 Navier-Stokes equations

Navier-Stokes equations for an incompressible, homogenous fluid can be written in this way:

$$\begin{cases} \rho_f \dfrac{D\boldsymbol{u}_f}{Dt} + \nabla \cdot \boldsymbol{T}_f(\boldsymbol{u}_f, p) = \boldsymbol{f}_f \quad in\ [0,T] \times \Omega_f^t \\ \\ \nabla \cdot \boldsymbol{u}_f = 0 \qquad\qquad\qquad\qquad in\ [0,T] \times \Omega_f^t. \end{cases} \tag{2.1}$$

[1] Reynold's Number is an adimensional quantity defined as $Re = \frac{\rho U L}{\mu}$ where ρ is the fluid density, U the velocity of the fluid, L a characteristic lenght (in our case vessel's diameter) and μ the dynamic viscosity. Usually if $Re < 4 \cdot 10^3$ it can be assumed the flow is not turbulent

The first of (2.1) come from momentum conservation, while the second, also called the continuity equation, represents the mass conservation.

Ω_f^t is the domain of the fluid problem at the time instant t, $\boldsymbol{u}_f$ is the fluid velocity vector, ρ_f is the density of the fluid (assumed constant with time), $\boldsymbol{f}_f$ an external force per unit of volume (usually gravity).

$\boldsymbol{T}_f$ is the fluid stress tensor, that for a Newtonian fluid can be written as a linear function of the velocity gradient:

$$\mathbf{T} = -p\mathbb{I} + \mu(\nabla \mathbf{u}_f + \nabla \mathbf{u}_f^t),$$

where p is the pressure, $\mathbb{I}$ the identity matrix and μ the *dinamic viscosity*, assumed constant. $\dfrac{D\boldsymbol{u}_f}{Dt}$ is called the material derivative. Its formulation depend of which formulation for the reference system is chosen.

Eulerian and Lagrangian formulation

In an *Eulerian* reference system the material derivative of a generic scalar function g is defined as:

$$\frac{Dg}{Dt} = \frac{\partial g}{\partial t} + \mathbf{u}_f \cdot \nabla g, \tag{2.2}$$

instead a *Lagrangian* reference system, the material derivative is written:

$$\frac{Dg}{Dt} = \frac{\partial g}{\partial t}. \tag{2.3}$$

The difference between the two systems is that in the (2.2) the attention is focused on one point in the domain and is computed the changing of the value of g in that point. Instead in the (2.3) the attention is pointed on the fluid particle that occupy a certain position at the initial time instant and is computed the value that g assume following the trajectory of the particle.

Eulerian Formulation is not suited for our puropose beacuse is characterized by a fixed frame, while we want a frame that follow the movement of the domain. Also *Lagrangian formulation* is not suited because is characterized by a frame following the fluid particles, while we want to keep fix the domain at the inlet and outlet sections.

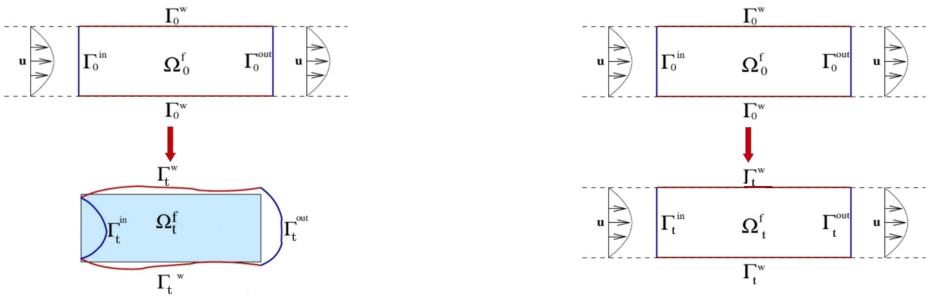

Figure 2.2: **Differences by Lagrangian** (left) **and Eulerian formulation**

One of the possible solutions of this problem is write the fluid equations in an *Arbitriarian Lagrangian Eulerian* (ALE) Formulation.

2.1.2 Arbitrarian Lagrangian Eulerian formulation of Navier-Stokes equations

Let $\mathcal{A}_t$ be a map which at each $t \in [0, T]$ associates a point $\tilde{\boldsymbol{x}}$ of the *reference configuration* $\widetilde{\Omega}_f$ (the domain configuration at time $t = 0$) to a point $\boldsymbol{x}$ in the current configuration Ω_f^t,

$$\mathcal{A}_t : \widetilde{\Omega}_f \subset \mathbb{R}^3 \to \Omega_f^t \subset \mathbb{R}^3, \qquad \boldsymbol{x}(\tilde{\boldsymbol{x}}, t) = \mathcal{A}_t(\tilde{\boldsymbol{x}}).$$

$\mathcal{A}_t$ is arbitrary, the only requirement is that it follows the moving interface. In our case the deformation of the domain is caused by the action that the fluit exert on the vessel but let's do an intermediate step and suppose to know the displacement $\boldsymbol{h} : \partial\widetilde{\Omega}_f \to \partial\Omega_f^T$ of the moving boundary. In order to reconstruct the fluid domain displacement $\widetilde{\boldsymbol{\eta}}_m$ also the internal points, we consider an harmonic extension of the the datum $\boldsymbol{h}$. *Given* $\widetilde{\Omega}_f$ *and* $\boldsymbol{h}$*, find* $\widetilde{\boldsymbol{\eta}}_m : \Omega \to \Omega_f^T$ *such that*

$$\begin{cases} -\Delta\widetilde{\boldsymbol{\eta}}_m = 0 & \text{in} \quad \widetilde{\Omega}_f, \\ \widetilde{\boldsymbol{\eta}}_m = \boldsymbol{h} & \text{on} \quad \partial\widetilde{\Omega}_f. \end{cases} \tag{2.4}$$

The fluid domain points are moved accordingly to 2.4

$$\boldsymbol{x} = \widetilde{\boldsymbol{x}} + \widetilde{\boldsymbol{\eta}}_m,$$

and we can also find fluid domain velocity

$$\boldsymbol{u}_m = \frac{\partial\widetilde{\boldsymbol{\eta}}_m}{\partial t}.$$

Let $v : \Omega_f^t \times [0,T] \to \mathbb{R}$ be a function living in the n the current fluid configuration and $\widetilde{v} := v \circ \mathcal{A}_t$ the corresponding function on the reference configuration, defined as

$$\widetilde{v} : \widetilde{\Omega}_f \times [0,T] \to \mathbb{R}, \quad \widetilde{v}(\tilde{\boldsymbol{x}}, t) := v(\mathcal{A}_t(\tilde{\boldsymbol{x}}), t).$$

The symbol $\dfrac{D^A}{Dt}$ will indicate the time derivative on the ALE frame, written in the spatial coordinates. It is defined as

$$\frac{D^A v}{Dt} : \Omega_f^t \times [t_0, T] \to \mathbb{R},$$

Using the classical rule to the time derivative, we have the following relation for a given function w

$$\frac{D^A w}{Dt} = \frac{\partial w}{\partial t} + \frac{D^A \boldsymbol{x}}{Dt} \cdot \nabla w = \frac{\partial w}{\partial t} + \boldsymbol{u}_m \cdot \nabla w. \tag{2.5}$$

In Eulerian formulation the conservation of momentum law is the following:

$$\rho_f \frac{\partial \boldsymbol{u}_f}{\partial t} + \rho_f (\boldsymbol{u}_f \cdot \nabla)\boldsymbol{u}_f + \nabla \cdot \boldsymbol{T}_f(\boldsymbol{u}_f, p) = \boldsymbol{f}_f, \tag{2.6}$$

but going to (2.5) we can write $\dfrac{\partial \boldsymbol{u}_f}{\partial t} = \dfrac{D^A \boldsymbol{u}_f}{Dt} - \boldsymbol{u}_m \cdot \nabla \boldsymbol{u}_f$ so substituting this in (2.3) the Navier-Stokes equations in ALE formulation read:

$$\begin{cases} \rho_f \dfrac{D^A \boldsymbol{u}_f}{Dt} + \rho_f((\boldsymbol{u}_f - \boldsymbol{u}_m) \cdot \nabla)\boldsymbol{u}_f + \nabla \cdot \boldsymbol{T}_f(\boldsymbol{u}_f, p) = \boldsymbol{f}_f & in\ [0,T] \times \Omega_f^t \\ \nabla \cdot \boldsymbol{u}_f = 0 & in\ [0,T] \times \Omega_f^t. \end{cases} \tag{2.7}$$

Equations (2.4) must be supplied with initial conditions for the velocity field

$$\boldsymbol{u}_f(\boldsymbol{x}, 0) = \boldsymbol{u}_{f,0} \qquad \text{in} \quad \widetilde{\Omega}_f,$$

and suitable boundary conditions. Let the boundary $\partial\Omega_f^t$ be splitted into two non-overlapping parts $\partial\Omega_f^t = \Gamma_{f,D}^t \cup \Gamma_{f,N}^t$. We will consider the following boundary conditions

$$\begin{cases} \boldsymbol{u}_f = \boldsymbol{\phi}_f & \text{on} \quad \Gamma_{f,D}^t, \\ \boldsymbol{T}_f \cdot \boldsymbol{n} = \boldsymbol{\psi}_f & \text{on} \quad \Gamma_{f,N}^t, \end{cases}$$

where $\boldsymbol{n}$ is the unit outward normal vector to $\partial\Omega_f^t$ and $\boldsymbol{\phi}_f$ and $\boldsymbol{\psi}_f$ are two given data with enough regularity.

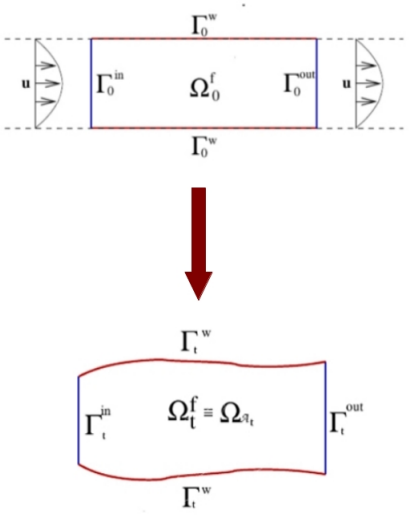

Figure 2.3: **ALE formulation**. The ALE frame described by map $\mathcal{A}_t$ which introduces a (fixed) frame of reference which is mapped at every time to the desired physical domain

2.2 Finite elasticity equations

Blood vessels' walls have a complex structure and the development of a mathematical model for describe their mechanical behaviour can be quite difficult. Their structure is composed by some layers with different caracteristic [12] :

- **Tunica intima** or **endothelium** is the more internal layer. is composed by cells that act as a "sensor" of the stress and secrete substances that control wall's composition.

- **Tunica media** is made by muscle cells circumferentially oriented, elastics fibers to permit distentions and collagen to guaratee resistance.

- **Tunica extrema** or **Adventia**, made of fibroblasts and collagen having again the purpose of increase mechanical resistance.

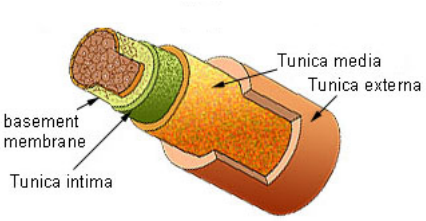

Figure 2.4: **Artery section**. The artery wall is made by different layers

It is quite impossibile reproduce in laboratory the exact behaviour of the vessels wall: first of all because they are made by muscle living tissue, then experiments with dead tissue can give results not totally exact but also because their beahviour is also function of the surrounding tissue, impossible to reproduce [17].

Is necessary then to use a model that is at the same time realistic and not too difficult to solve. Since we are treating large deformation we modeled the structure using the equations of finite elasticity, while for the reology of the material of the vessel a non-linear, exponential elasticity constitutive law has been used. The conservation of momentum law in Lagrangian formulation reads as follow:

$$\frac{\partial^2 \widetilde{\boldsymbol{\eta}}_s}{\partial t^2} - \nabla \cdot \widetilde{\boldsymbol{T}}_s(\widetilde{\boldsymbol{\eta}}_s) = \boldsymbol{f}_s \quad in\ (0,T) \times \widetilde{\Omega}_s^0, \tag{2.8}$$

$\widetilde{\Omega}_s^0$ is the reference configuration of the structure. $\widetilde{\boldsymbol{\eta}}_s$ represent the displacement, defined as:

$$\widetilde{\boldsymbol{\eta}}_s(\widetilde{\boldsymbol{x}}, t) = \boldsymbol{x}(\widetilde{\boldsymbol{x}}, t) - \widetilde{\boldsymbol{x}},$$

$\boldsymbol{x}(\widetilde{\boldsymbol{x}}, t)$ being the vector that identify the position at the time instant t of the point that in the reference configuration occupy the position $\widetilde{\boldsymbol{x}}$. $\widetilde{\boldsymbol{T}}_s$ is called the *Piola-Kirchoff* stress tensor and it's linked to the Cauchy stress tensor by the relation:

$$\widetilde{\boldsymbol{T}}_s = J\boldsymbol{T}_s\boldsymbol{F}^{-T},$$

where

$$\boldsymbol{F} = \widetilde{\nabla}\widetilde{\boldsymbol{\eta}}_{\boldsymbol{s}} + \mathbb{I}$$
$$J = det(\boldsymbol{F}),$$

$\boldsymbol{F}$ is called deformation gradient. Then a relation linking $\widetilde{\boldsymbol{\eta}}_{\boldsymbol{s}}$ to $\widetilde{\boldsymbol{T}}_s$ is needed. This relation is called *Constitutive law* of the material. An exponential relation has been choosed, whose expression is the following [16]:

$$\widetilde{\boldsymbol{T}}_s = \alpha J^{\frac{2}{3}}(\boldsymbol{F} - \frac{1}{3}tr(\boldsymbol{C})\boldsymbol{F}^{-T})e^{\gamma(J^{\frac{2}{3}}tr(\boldsymbol{C})-3)} + \frac{\kappa}{2}(J - 1 + \frac{1}{J}lnJ)J\boldsymbol{F}^{-T},$$

where

$$\boldsymbol{C} = \boldsymbol{F}^T\boldsymbol{F},$$

and κ and α are respectively the *bulk modulus* and the *shear modulus*. For small deformations such material behaves as a linear structure described by the infinitesimal elasticity, characterized by a Poisson's ratio ν and a Young modulus E related to κ and α as follows

$$\kappa = \frac{E}{3(1-2\nu)}, \qquad \alpha = \frac{E}{2(1+\nu)}.$$

The parameter γ is peculiar of this kind of material and tunes the stiffness for large displacements.

2.3 Coupled Fluid-Structure interaction (FSI) problem

A fluid-structure interaction (FSI) problem arises when a consistent amount of energy is exchanged between a fluid and a structure. The study of FSI problems has important applications in biomechanics but also in the design of many engineering systems, e.g. aircraft and bridges.

In the case here treated here we consider the mutual interaction between the blood and an arterial vessel. One of the most important features of blood flow in arteries is its unsteadiness, or, more precisely, pulsatility. We can identify two phases: during the systole, that in physiological cases occupies one third of the whole cardiac cycle, blood pressure rise and reach its maximum (in normal situations between 90 and 120 mmHg), due to the contaction of heart's left ventricle. During this phase the vessel's wall deformation accumulates part of the mechanical energy as elastic energy, which will afterwards be returned back to the blood during the diastole , the phase in which blood pressure decrease and reach its basis level (normally between 60 and 80 mmHg). This blood-vessel interaction mechanism is very important because allows to keep almost uniform values of blood's velocity and pressure at capillary level [13].

There are two possible ways to made a mathematical model for the FS interaction in arteries:

$\Rightarrow$ In a *Global approach* arteries are described as a whole continuum that includes the innermost fluid region and the outer solid wall. The mathematical complexity, combined with the high computing power requested by this model generally go beyond the realistic possibilities offered by present day computer simulations[13];

$\Rightarrow$ In a *Coupled approach* we consider two different submodels, one for fluid, another one for the structure, togheter with suitable matching conditions which play the role of boundary conditions of the submodels.

We have here considered a Coupled approach using the models that have been exposed in the previous pages: the Navier-Stokes equations written in ALE formulation for the fluid problems, the equations of finite elasticity for the structure problem and the harmonic extension for the fluid domain problem. There is no structure domain problem since it coincides with the structure problem itself, since it has been written in Lagrangian formulation. From the mathematical viewpoint the problem is very challenging due to its nonlinear nature.

The conditions that link structure and fluid problem have to be physically consistent but also ensure the well posedness of the mathematical problem, indeed although each submodel yiedls a stable problem it is no guaranteed that the global problem is stable too[13]. The linking conditions that have been used are:

Physical interface continuity

1. the fluid and the structure particles have to share the same velocity at the FS interface (no-slip condition) $\rightarrow \boldsymbol{u}_f = \dfrac{\partial \boldsymbol{\eta_s}}{\partial t}$ on Γ^t

2. the fluid and the structure have to extert the same normal stresses at the FS interface (third Newton's law) $\rightarrow \boldsymbol{T}_s \cdot \mathbf{n} = \boldsymbol{T}_f \cdot \mathbf{n}$ on Γ^t

where $\Gamma^t = \Omega_f^t \cap \Omega_s^t$ and $\mathbf{n}$ is the local normal vector of Γ^t exiting from the fluid domain.

Geometrical interface continuity

The fluid and structure domains have to share to same displacement at the FS interface $\rightarrow \widetilde{\boldsymbol{\eta}}_m = \widetilde{\boldsymbol{\eta}}_s$ on $\widetilde{\Gamma}$, where $\widetilde{\Gamma} = \widetilde{\Omega}_f \cap \widetilde{\Omega}_s$.

Then the strong formulation of the FSI problem reads: find fluid velocity

$\boldsymbol{u}_f$, fluid pressure $\boldsymbol{p}_f$, fluid domain displacement $\boldsymbol{\eta}_m$ and structure displacement $\boldsymbol{\eta}_s$ such that:

$$\begin{cases} \rho_f \dfrac{D^A \boldsymbol{u}_f}{Dt} + \rho_f((\boldsymbol{u}_f - \boldsymbol{u}_m)\cdot\nabla)\boldsymbol{u}_f + \nabla\cdot\boldsymbol{T}_f(\boldsymbol{u}_f, p) = \boldsymbol{f}_f & in\ [0,T]\times\Omega_f^t \\ \nabla\cdot\boldsymbol{u}_f = 0 & in\ [0,T]\times\Omega_f^t \\ \dfrac{\partial^2\widetilde{\boldsymbol{\eta}}_s}{\partial t^2} - \nabla\cdot\widetilde{\boldsymbol{T}}_s(\widetilde{\boldsymbol{\eta}}_s) = \mathbf{f}_s & in\ [0,T]\times\widetilde{\Omega}_s^0 \\ \boldsymbol{u}_f = \dfrac{\partial\boldsymbol{\eta_s}}{\partial t} & on\ [0,T]\times\Gamma^t \\ \boldsymbol{T}_s\cdot\mathbf{n} = \boldsymbol{T}_f\cdot\mathbf{n} & on\ [0,T]\times\Gamma^t \\ -\Delta\widetilde{\boldsymbol{\eta}}_m = 0 & in\ [0,T]\times\widetilde{\Omega}_f \\ \widetilde{\boldsymbol{\eta}}_m = \widetilde{\boldsymbol{\eta}}_s & on\ [0,T]\times\widetilde{\Gamma}, \end{cases} \tag{2.9}$$

To solve the problem are also necessaries suitable initial and boundary conditions on $(\delta\Omega_s \cup \delta\Omega_f \setminus \Gamma)$.

Nonlinear behaviour of the problem is due to the convective term of $(2.9)_1$ and the non-linear constitutive law chosed for $\widetilde{\boldsymbol{T}}_s$ in equation $(2.9)_3$. Moreover, since the interface position of the fluid domain must coincide with the solid position at the interface, that is unknown since it depends on the interaction between the two subproblems, introduce a source of non-linearity known as *geometrical coupling* [16].

Although many reasonable simplification have been adopted both for defininion of the fluid and structure problem , find an analitical solution of the FSI coupled problem is not possible. Therefore we have to discretize the problem in space and in time. This will be made using *Finite Element Method* and *Backward Euler Method*. Moreover we need to introduce an algorithm that decouple the structure and fluid subproblems and treat the nonlinearities that are present. These will be the topics of the next chapter.

Chapter 3

Numerical discretization

As we have seen in the previous chapter the FSI problem can be written as a system of partial differential equations (PDE). In general it is not possible to find an analitical solution of PDE so it is necessary to use numerical methods. The problems we have to face are the following:

- Discretize the problem with respect to space variables: this will be made by using the Finite Element Method (FEM). In section 3.1 will be made an introduction to this mehod.
- Discretize the problem with respect to time variable: this will be made using the finite difference method, in particular using the backward Euler method. This will be presented in section 3.2.
- At each timestep solve the non linear FSI problem handling the physical and geometrical interface conditions togheter with the constituitive non-linearities present in the fluid and structure subproblems. The algorithm chosen to solve this problem will be presented in section 3.3.

3.1 A brief introduction to the FEM

The *finite element method* is a numerical technique for finding approximate solutions to partial differential equations (PDE) and their systems. FEM is a special case of the more general Galerkin method with polynomial approximation functions. With FEM we get an approximate solution of PDE by means of a system of algebraic equations for steady state problems or system of ordinary differential equations for transient problems (this last is our case, where temporal derivatives will be approximated through finite differences). In this section we are going to take as an example a very simple differential

problem, the Poisson's equation with a Dirichlet condition, just to explain briefly FEM . See [19] for further details.

The model problem is: Find $u(x_1, x_2)$ so that

$$\begin{cases} -\Delta u = f & in\ \Omega, \\ u = 0 & on\ \partial\Omega, \end{cases} \tag{3.1}$$

where $\Omega \subset \mathbb{R}^2$ is a limited domain and $\partial\Omega$ his boundary. This formulation of the problem is in general not suitable for the numerical solution. Indeed it can be showed that also if physical solutions of a problem modeled by (3.1) may exist, it can be not C^2, so that the Laplace operator in (3.1) would not take sense. To make an example of this problem we reduce our tractation to a 1D problem

$$\begin{cases} -u'' = f(x), & 0 < x < 1, \\ u(0) = 0, & u(1) = 0. \end{cases} \tag{3.2}$$

This problem represents the displacement of a a wire fixed at his sides, with a unitary tension, in the hypothesis of little displacement, with f that represent the force perpendicular to the wire for unit lenght. We can imagine now that f is defined as:

$$f(x) = \begin{cases} 0 & \text{if } \ x < 0.4, \ x > 0.6 \\ 1 & \text{if } \ 0.4 < x < 0.6, \end{cases}$$

a solution of the problem exist and is the following:

$$u(x) = \begin{cases} -\dfrac{1}{10}x & \text{if } x \in [0, 0.4], \\ \dfrac{1}{2}x^2 - \dfrac{1}{2}x - \dfrac{2}{25} & \text{if } x \in [0.4, 0.6], \\ -\dfrac{1}{10}(1-x) & \text{if } x \in [0.6, 1], \end{cases}$$

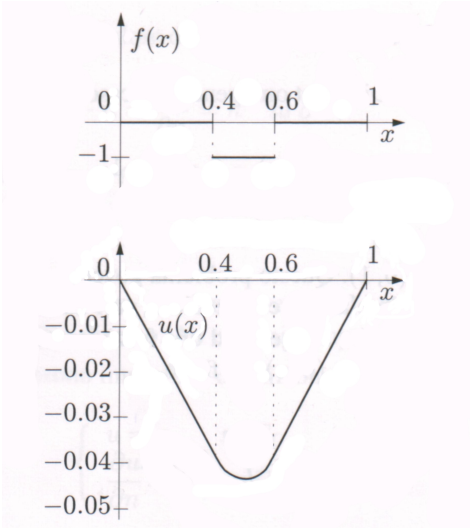

Figure 3.1: The solution of the problem (3.2) with the condition (3.1) (displayed above)

As we can see the solution is only C^1. This is because in our example $f \notin C^0$. We need then to introduce a different formulation that is called *Weak formulation* ((3.1) and (3.2) are called *Strong formulation*) to extend the validity of the problem. *Weak formulation* will also be useful for the numerical discretization.

3.1.1 Weak formulation of the Poisson's problem

We multiply every term of the first equation of $(3.1)_1$ for an arbitrary function v, that we call test function, and we integrate on all Ω to obtain:

$$-\int_\Omega \Delta u v = \int_\Omega f v \tag{3.3}$$

We need now to manage (3.3) to eliminate the second order derivative, so the solution will require less regularity (in this way the solution will need to be only C^1 and not C^2). Green's formula say that we can write:

$$-\int_\Omega \Delta u v \; d\Omega = \int_\Omega \nabla u \cdot \nabla v \; d\Omega - \int_{\partial\Omega} \frac{\partial u}{\partial n} v \; d\gamma.$$

Since we are solving a homogeneous Dirichlet problem, we choose only test functions that vanish on $\partial\Omega$, so that we can write this weak formulation for problem (3.1):

$$\text{find } u \in V: \qquad \int_\Omega \nabla u \cdot \nabla v \; d\Omega = \int_\Omega f v \; d\Omega \qquad \forall v \in V, \tag{3.4}$$

having defined the following functional spaces:

$$L^2(\Omega) = \{g : \Omega \to \mathbb{R} : \int_\Omega g^2 d\Omega < +\infty\},$$

$$H^1(\Omega) = \{v : \Omega \to \mathbb{R} : v \in L^2(\Omega), \frac{\partial v}{\partial x_i} \in L^2(\Omega),\ i = 1, 2\},$$

$$V = H_0^1(\Omega) = \{v \in H^1(\Omega) : v = 0 \text{ on } \delta\Omega\}.$$

It is possible to show that by requiring that (3.4) is satisfied for all $v \in V$ the solution of (3.4) coincides with that of (3.1) for regular data. However, with (3.4) it is required that $f \in L^2(\Omega)$, no more $f \in C^0(\Omega)$ as for (3.1). Then the weak formulation extends the strong formulation to cases as the one described in the previous section. Moreover it is the starting point to build the FEM system. We can rewrite 3.4 introducing the following notations:

$$a : V \times V \to \mathbb{R}, \quad a(u, v) = \int_\Omega \nabla u \cdot \nabla v \ d\Omega,$$

$$F : V \to \mathbb{R}, \quad F(v) = \int_\Omega f v \ d\Omega,$$

So that the problem can be written as:

$$\text{find } u \in V : \qquad a(u, v) = F(v) \qquad \forall v \in V. \tag{3.5}$$

3.1.2 The Galerkin's problem

We now define $V_h \subset V$ as family of functional spaces dependent on a positive parameter h so that $\dim V_h = N_h < \infty$ and $\lim_{h\to 0} V_h = V$. This mean that every function of V_h space can be written as a linear combination of N_h basis $\{\varphi_j, j = 1 \dots N_h\}$. We can now approximate the problem reducing the functional space in which we are searching its solution just to V_h and write:

$$\text{find } u_h \in V_h : \qquad a(u_h, v_h) = F(v_h) \qquad \forall v_h \in V_h. \tag{3.6}$$

We observe that we need only that (3.6) has to be satisfied for every basis function of V_h because every other function of V_h can be written as linear combination of the basis functions. Then we can rewrite te problem as:

$$a(u_h, \varphi_i) = F(\varphi_i),\ i = 1, 2, \dots, N_h. \tag{3.7}$$

But since $u_h \in V_h$, we have

$$u_h(\boldsymbol{x}) = \sum_{j=1}^{N_h} u_j \varphi_j(\boldsymbol{x}), \tag{3.8}$$

where $u_j, j = 1, \ldots, N_h$, are the unknown coefficients. The problem become:

$$\sum_{j=1}^{N_h} u_j a(\varphi_j \varphi_i) = F(\varphi_i), \ i = 1, 2, \ldots, N_h. \tag{3.9}$$

Now we denote with: A the matrix with elements $a_{ij} = a(\varphi_i, \varphi_j)$, with $\boldsymbol{u}$ the vector that has for components the unknown coefficients u_j and with $\boldsymbol{f} = [f_i]$ the vector with components $f_i = F(\varphi_i)$. Then equation (3.9) can be rewritten as the following linear sistem:

$$A\boldsymbol{u} = \boldsymbol{f}. \tag{3.10}$$

3.1.3 Solution of the Poisson's problem with FEM

Coming back to the specific case of the Poisson's problem, this can be rewritten as:

$$\text{find } u_h \in V_h : \qquad \int_\Omega \nabla u_h \cdot \nabla v_h \, d\Omega = \int_\Omega f v_h \, d\Omega \qquad \forall v_h \in V_h$$

We can imagine now to find in the domain Ω some points, that we'll call nodes $\boldsymbol{N}_j$ with $i = 1, \ldots, N_h$. From this descent that a basis of the V_h space can be imaginated as the set of the $\varphi_j \in V_h, j = 1, \ldots, N_h$ so that:

$$\varphi_j(\boldsymbol{N}_i) = \delta_{ij} = \begin{cases} 0 \ i \neq j \\ 1 \ i = j \end{cases}$$

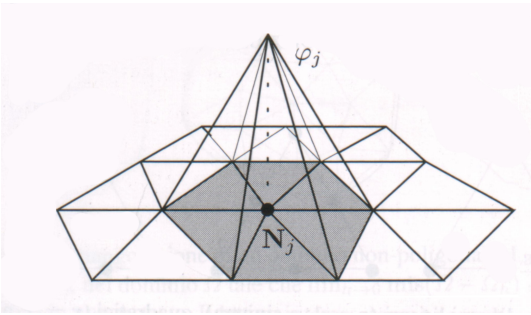

Figure 3.2: A basis function φ_j

Thanks to (3.9) we can then write the problem as the following linear sistem:

$$\sum_{j=1}^{N_h} u_j \int_\Omega \nabla\varphi_j \cdot \nabla\varphi_i \, d\Omega = \int_\Omega f\varphi_i \, d\Omega \; i = 1, \ldots, N_h. \tag{3.11}$$

Then the matrix and and the vector of (3.10) in this specific case are:

$$A = [a_{ij}] \text{ with } a_{ij} = \int_\Omega \nabla\varphi_j \cdot \nabla\varphi_i \, d\Omega$$

$$\boldsymbol{u} = [u_j] \text{ with } u_j = u_h(\boldsymbol{N}_j), \;\; \boldsymbol{f} = [f_j] \text{ with } f_j = \int_\Omega f\varphi_i \, d\Omega.$$

It can be demonstrated that if:

$$\lim_{h\to 0} \inf_{v_h \in V_h} \|v - v_h\| = 0 \qquad \forall v \in V,$$

FEM converge to the exact solution u, that is:

$$\lim_{h\to 0} \|u - u_h\| = 0.$$

It is important to notice that since the PDE we want to solve is linear [1] then we obtained a linear system. If the PDE is non-linear the system is non-linear, and this will be our case.

3.2 Discretization of the problem in time

In the previous section we show the FEM formulation of the Poisson problem, that is independent of time. In our problem instead time derivatives appears, so we need to find before a way to approximate them and have a problem that contain only space derivatives. Let write the strong formulation of the

[1] a PDE is defined linear when it depends lineary from the unkonwn function and its derivatives

problem, as seen in chapter 2.

$$\begin{cases} \rho_f \dfrac{D^A \boldsymbol{u}_f}{Dt} + \rho_f((\boldsymbol{u}_f - \boldsymbol{u}_m)\cdot\nabla)\boldsymbol{u}_f + \nabla\cdot\boldsymbol{T}_f(\boldsymbol{u}_f, p) = \boldsymbol{f}_f & in\ [0,T]\times\Omega_f^t \\ \nabla\cdot\boldsymbol{u}_f = 0 & in\ [0,T]\times\Omega_f^t \\ \dfrac{\partial^2\widetilde{\boldsymbol{\eta}}_s}{\partial t^2} - \nabla\cdot\widetilde{\boldsymbol{T}}_s(\widetilde{\boldsymbol{\eta}}_s) = \mathbf{f}_s & in\ [0,T]\times\widetilde{\Omega}_s^0 \\ \boldsymbol{u}_f = \dfrac{\partial\boldsymbol{\eta_s}}{\partial t} & on\ [0,T]\times\Gamma^t \\ \boldsymbol{T}_s\cdot\mathbf{n} = \boldsymbol{T}_f\cdot\mathbf{n} & on\ [0,T]\times\Gamma^t \\ -\Delta\widetilde{\boldsymbol{\eta}}_m = 0 & in\ [0,T]\times\widetilde{\Omega}_f \\ \widetilde{\boldsymbol{\eta}}_m = \widetilde{\boldsymbol{\eta}}_s & on\ [0,T]\times\widetilde{\Gamma}. \end{cases} \tag{3.12}$$

The choice that have been made for approximate time derivatives is to use *Backward Euler Method*. This method requires to split time domain $[0,T]$ in n intervals of lenght Δt. We can identify then $n+1$ time istants, the generic one can be written as $t^n = n\Delta t$, $n = 0,\ldots,n+1$. *Backward Euler Method* approximates a function time derivative at the the instant $n+1$ using the values assumed by the function at the previous time instants [4]. If $\boldsymbol{u}_f^{n+1}$ and $\widetilde{\boldsymbol{\eta}}_s^{n+1}$ are the approximated values of the fluid velocity and structure displacement at the instant $n+1$ we can define:

$$\frac{D^A\boldsymbol{u}_f}{Dt} := \frac{\boldsymbol{u}_f^{n+1} - \boldsymbol{u}_f^n}{\Delta t},$$

$$\frac{\partial\boldsymbol{\eta}_s}{\partial t} := \frac{\boldsymbol{\eta}_s^{n+1} - \boldsymbol{\eta}_s^n}{\Delta t},$$

$$\frac{\partial^2\widetilde{\boldsymbol{\eta}}_s}{\partial t^2} := \frac{\widetilde{\boldsymbol{\eta}}_s^{n+1} - 2\widetilde{\boldsymbol{\eta}}_s^n + \widetilde{\boldsymbol{\eta}}_s^{n-1}}{\Delta t^2},$$

and write the strong formulation of the time discrete problem:

Fluid-Structure problem

Given the (unknown) fluid domain velocity $\boldsymbol{u}_m^{n+1}$ and fluid domain Ω_f^{n+1}, the solution at previous time steps, and functions $\boldsymbol{f}_f^{n+1}$, $\boldsymbol{f}_s^{n+1}$, find fluid velocity

$\boldsymbol{u}_f^{n+1}$, pressure p_f^{n+1} and structure displacement $\widetilde{\boldsymbol{\eta}}_s^{n+1}$ such that

$$\begin{cases} \rho_f \dfrac{\boldsymbol{u}_f^{n+1}}{\Delta t} + \rho_f((\boldsymbol{u}_f^{n+1} - \boldsymbol{u}_m^{n+1}) \cdot \nabla)\boldsymbol{u}_f^{n+1} + \nabla \cdot \boldsymbol{T}_f(\boldsymbol{u}_f^{n+1}, p_f^{n+1}) = \boldsymbol{f}_f^{n+1} + \rho_f \dfrac{\boldsymbol{u}_f^n}{\Delta t} & \text{in } \Omega_f^{n+1}, \\ \nabla \cdot \boldsymbol{u}_f^{n+1} = 0 & \text{in } \Omega_f^{n+1}, \\ \rho_s \dfrac{\widetilde{\boldsymbol{\eta}}_s^{n+1}}{\Delta t^2} - \nabla \cdot \widetilde{\boldsymbol{T}}_s(\widetilde{\boldsymbol{\eta}}_s^{n+1}) = \widetilde{\boldsymbol{f}}_s^{n+1} + \rho_s \dfrac{2\widetilde{\boldsymbol{\eta}}_s^n - \widetilde{\boldsymbol{\eta}}_s^{n-1}}{\Delta t^2} & \text{in } \widetilde{\Omega}_s, \\ \boldsymbol{u}_f^{n+1} = \dfrac{\boldsymbol{\eta}_s^{n+1} - \boldsymbol{\eta}_s^n}{\Delta t} & \text{on } \Gamma^{n+1}, \\ \boldsymbol{T}_s^{n+1}(\boldsymbol{\eta}_s^{n+1})\,\mathbf{n} = \boldsymbol{T}_f^{n+1}(\boldsymbol{u}_f^{n+1}, p_f^{n+1})\,\mathbf{n} & \text{on } \Gamma^{n+1}, \end{cases} \tag{3.13}$$

Geometry problem

Given the (unknown) interface structure displacement $\widetilde{\boldsymbol{\eta}}_s$ solve a harmonic extension problem

$$\begin{cases} -\Delta\widetilde{\boldsymbol{\eta}}_m^{n+1} = 0 & in\ [0,T] \times \widetilde{\Omega}_f \\ \widetilde{\boldsymbol{\eta}}_m^{n+1} = \widetilde{\boldsymbol{\eta}}_s^{n+1} & on\ [0,T] \times \widetilde{\Gamma}. \end{cases} \tag{3.14}$$

and then find accordingly the discrete fluid domain velocity $\widetilde{\boldsymbol{u}}_m^{n+1}$ and the points $\boldsymbol{x}_f^{n+1}$ of the new fluid domain by

$$\widetilde{\boldsymbol{u}}_m^{n+1} := \frac{\boldsymbol{\eta}_m^{n+1} - \boldsymbol{\eta}_m^n}{\Delta t}, \qquad \boldsymbol{x}_f^{n+1} = \widetilde{\boldsymbol{x}}_f + \widetilde{\boldsymbol{\eta}}_m^{n+1}.$$

Backward Euler Method is a first order numerical method [4]. That is:

$$\left\| \frac{\partial \boldsymbol{u}_f}{\partial t}(t^n, \boldsymbol{x}) - \frac{\boldsymbol{u}_f^n(\boldsymbol{x}) - \boldsymbol{u}_f^{n-1}(\boldsymbol{x})}{\Delta t} \right\| = \mathcal{O}(\Delta t)$$

$$\left\| \frac{\partial^2 \widetilde{\boldsymbol{\eta}}_s}{\partial t^2}(t^n, \boldsymbol{x}) - \frac{\widetilde{\boldsymbol{\eta}}_s^n(\boldsymbol{x}) - 2\widetilde{\boldsymbol{\eta}}_s^{n-1}(\boldsymbol{x}) + \widetilde{\boldsymbol{\eta}}_s^{n-2}(\boldsymbol{x})}{\Delta t^2} \right\| = \mathcal{O}(\Delta t)$$

3.3 Partioned Algorithms for the Numerical Solution

We are here interested in partitioned algorithms for the numerical solution of the FSI problem, which consist in the successive solution of the three subproblems in an iterative framework. The main problem we have to solve are:

1. The treatment of the geometrical interface condition, which enforces the continuity of displacements at the FS interface between the fluid and the structure domains;

2. The treatment of the constitutive non-linearities featured by the fluid and the structure problems separately;

3. The treatment of the physical interface conditions, which enforce the continuity of velocities and normal stresses at the fluid-structure interface.

As will be showed in the next pages, the choice that have been made for every instant of time is to make two iterative cycles: one external cycle that treat togheter points 1 and 2 and one internal cycle for point 3, that is the more critical, due to a phenomenon know as added-mass effect [14]. This phenomenon made that the convergence for an iterative cycle of a FSI problem is slow if the densities of the fluid and the structure are the very similar, as in our case. The convergence properties of the double-loop scheme can be improved using Robin boundary condition at the fluid-structure interface [9]. Moreover, when the densities are similar, it is not possible to consider explicit coupling, so that the pysical interface conditions have to be imposed exactly through an implicit treatment.

3.3.1 The double-loop iteration scheme

We now expose the double-loop iteration scheme with we have used to solve the FSI problem. To do this we indroduce the following operators (time index has been omitted):

- $\mathcal{S}(\widetilde{\boldsymbol{\eta}}_s)$ to define the structure problem
- $\mathcal{F}(\boldsymbol{u}_f - \boldsymbol{u}_m)$ to define the fluid problem
- $\mathcal{H}$ to define the harmonic extension problem
- $\mathcal{G}_f$ and $\mathcal{G}_s$ to define the forcing terms rispectively in the fluid and the structure problem

We can notice that the fluid and structure problem operators depends on the variables that we want calculate, highlighting the fact that these problems are non-linear. Using the introduced operators the FSI problem can be rewritten in this way:

harmonic extension $\begin{cases} \mathcal{H}\widetilde{\boldsymbol{\eta}}_m = 0 & in\ \widetilde{\Omega}_f, \\ \widetilde{\boldsymbol{\eta}}_m = \widetilde{\boldsymbol{\eta}}_s & on\ \widetilde{\Gamma}, \end{cases}$

fluid problem $\mathcal{F}(\boldsymbol{u}_f - \boldsymbol{u}_m)\boldsymbol{v}_f = \mathcal{G}_f \quad in\ \Omega_f,$

structure problem $\mathcal{S}(\widetilde{\boldsymbol{\eta}}_s) = \mathcal{G}_s \quad in\ \widetilde{\Omega}_s,$

physical interface conditions $\begin{cases} \boldsymbol{u}_f = \boldsymbol{u}_s & in\ \Gamma, \\ \boldsymbol{T}_s \cdot \mathbf{n} = \boldsymbol{T}_f \cdot \mathbf{n} & in\ \Gamma, \end{cases}$

where $v_f := (\boldsymbol{u}_f, p_f)$ is a notation that we use to collect the fluid unknowns and $\boldsymbol{u}_s = \dfrac{\partial \boldsymbol{\eta}_S}{\partial t}$.

To solve the non-linearities present in the fluid and structure problem we introduce the Newton method, usually used to find the roots of a non linear real funtion $f(x)$, where x is also a real number. Newton method is based on a iterative cycle that reads:

$$f^{'}(x^{(k)})\delta x^{(k+1)} = -f(x^{(k)})$$

$$x^{(k+1)} = x^{(k)} + \delta x^{(k+1)}$$

We decide, for reasons that will be clear later, to combine linearly the two physical interface conditions, so that we obtain the following Robin-type boundary conditions:

$$\begin{cases} \alpha_f \boldsymbol{u}_f + \boldsymbol{T}_f \cdot \mathbf{n} = \alpha_f \boldsymbol{u}_s + \boldsymbol{T}_s \cdot \mathbf{n} \\ \alpha_s \boldsymbol{u}_s - \boldsymbol{T}_s \cdot \mathbf{n} = \alpha_s \boldsymbol{u}_f - \boldsymbol{T}_f \cdot \mathbf{n} \end{cases}$$

where $\alpha_f \neq \alpha_s$ are two parameters that will be discussed later. We can finally write the double-loop cycle:

External loop (index k)

Given the solution at iteration k, solve at the current iteration $k+1$ until convergence

(1) The harmonic extension

$$\begin{cases} \mathcal{H}\,\widetilde{\boldsymbol{\eta}}_m^{k+1} = 0 & \text{in } \widetilde{\Omega}_f \\ \widetilde{\boldsymbol{\eta}}_m^{k+1} = \widetilde{\boldsymbol{\eta}}_s^{k} & \text{on } \widetilde{\Gamma}, \end{cases}$$

obtaining the new fluid domain Ω_f^{k+1} *and the fluid domain velocity* $\boldsymbol{u}_m^{k+1}$.

(2) The linearized FSI problem in a known domain. For its solution, we consider the following partitioned algorithm:

Internal loop iterations (index l)

Given the solution at subiteration $l-1$*, solve at the current subiteration* l *until convergence.*

(a) The fluid subproblem with a Robin condition at the FS interface

$$\begin{cases} \nabla_{v_f}\mathcal{F}(\boldsymbol{u}_f^k - \boldsymbol{u}_m^{k+1})\,\boldsymbol{v}_{f,l}^{k+1} = \mathcal{G}_f & \text{in } \Omega_f^k \\ \alpha_f \boldsymbol{u}_{f,l}^{k+1} + \boldsymbol{T}_{f,l}^{k+1}\cdot\mathbf{n} = \alpha_f \boldsymbol{u}_{s,l-1}^{k+1} + \boldsymbol{T}_{s,l-1}^{k+1}\cdot\mathbf{n} & \text{on } \Gamma^{k+1} \end{cases}$$

(b) The structure subproblem with a Robin condition at the FS interface

$$\begin{cases} \nabla_{\eta_s}\mathcal{S}(\widetilde{\boldsymbol{\eta}}_s^k)\,\delta\widetilde{\boldsymbol{\eta}}_{s,l}^{k+1} = \mathcal{G}_s - \mathcal{S}(\widetilde{\boldsymbol{\eta}}_s^k) & \text{in } \widetilde{\Omega}_s \\ \alpha_s \boldsymbol{u}_{s,l}^{k+1} + \boldsymbol{T}_{s,l}^{k+1}\cdot\mathbf{n} = \alpha_s \boldsymbol{u}_{f,l}^{k+1} + \boldsymbol{T}_{f,l}^{k+1}\cdot\mathbf{n} & \text{on } \widetilde{\Gamma} \end{cases}$$

(c) Relaxation

$$\begin{cases} \widetilde{\boldsymbol{\eta}}_{s,l}^{k+1} = \omega\widetilde{\boldsymbol{\eta}}_{s,l}^{k+1} + (1-\omega)\widetilde{\boldsymbol{\eta}}_{s,l-1}^{k+1} \\ \widetilde{\boldsymbol{T}}_{s,l}^{k+1} = \omega\widetilde{\boldsymbol{T}}_{s,l}^{k+1} + (1-\omega)\widetilde{\boldsymbol{T}}_{s,l-1}^{k+1} \end{cases}$$

where $\omega \in (0,1)$.

We need then convergence criteria for both internal and external cycles. For the internal cycle we proceed until:

$$\|\widetilde{\boldsymbol{\eta}}_{s,l}^{k+1} - \widetilde{\boldsymbol{\eta}}_{s,l-1}^{k+1}\| + \|\boldsymbol{T}_{s,l}^{k+1}\cdot\mathbf{n} - \boldsymbol{T}_{s,l-1}^{k+1}\cdot\mathbf{n}\| < \epsilon_1,$$

while for the external cycle we have the following criteria, respectivly for the harmonic extensions:

$$\|\widetilde{\boldsymbol{\eta}}_m^{k+1} - \widetilde{\boldsymbol{\eta}}_m^k\| < \epsilon_2,$$

and for the non-linearities:

$$\|\boldsymbol{u}_f^{k+1} - \boldsymbol{u}_f^k\| + \|p_f^{k+1} - p_f^k\| < \epsilon_3,$$

$$\|\widetilde{\boldsymbol{\eta}}_s^{k+1} - \widetilde{\boldsymbol{\eta}}_s^k\| < \epsilon_4,$$

when the criteria of the external cycle are satisfied we can increment time index.

It is important to notice that the PDE's that appear in the external cycle are now all linear, because the operators that define the two problems have been linearized. This mean that they can be solved with FEM, as seen for the Poisson's equation in section 3.1, because they discretiziation lead now to a linear algebraic system.

The parameters α_s and α_f define the convergence properties of the double-loop algorithms. There are mathematical models that can define this parameters to guarantee convergence and maximize its velocity. It can be noticed that if $\alpha_f \to \infty$ and $\alpha_s \to 0$ we obtain the originary Dirichlet-Neumann scheme, with Dirichlet interface conditions for the fluid problem and Neumann interface conditions for the structure problem. This scheme is not suited because it needs a very small relaxation to guarantee convergence and this mean small convergence velocity [9]. This phenomenon is known because is responsible for the slow convergence of implicit Dirichlet-Neumann schemes in typical haemodynamic applications [14]. The cause have to be searched in the fact that we have considered blood as an incompressible fluid and in the fact that $\rho_f \approx \rho_s$ [8] (blood, as all human tissues is made mainly by water). If we use a Robin-Robin scheme, that mean to impose Robin type interface conditions both for the fluid and structure problem, no relaxation is needed, and this mean that the convergence velocity is appreciably higher [9].

Chapter 4

A clinical application

In this chapter a possible application of the mathematical tools explained in the previous sections will be showed: the simulation of the fluid dynamics in a real human carotid affected by atherosclerosis. A short introduction to what is atherosclerosis will be made in section 4.1. We will explain the problems it poses to health and how it affect the geometry and the mechanical characteristics of arteries. In section 4.2 we will discuss the choice of the initial and boundary parameters necessary to define the simulations and the sensitivity of the numerical solution respect to the discretization chosen for the domain. In section 4.3 we will expose the results obtained by the simulations of a carotid before and after a surgical operation of atherosclerotic plaque removal, highlighting the differences in important parameters in the two cases. Finally in section 4.4 there is a brief summary of the main results obtained.

4.1 Introduction to Atherosclerosis

Atherosclerosis is a disease of arteries which results in a reduction of lumen area (stenosis) and vessel's wall thickening and stiffening caused mainly by a build up of fatty material in the artery wall. This disease causes in general a decrease of blood flow through the diseased artery [7].

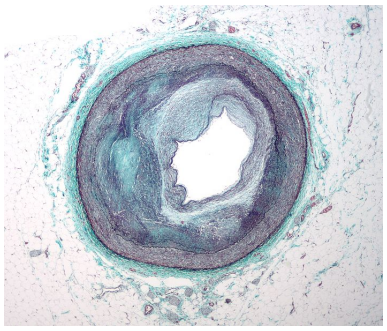

Figure 4.1: **Stenosis**. In this micrograph of a coronary artery is very evident the reduction in lumen

Atherosclerotic disease of the carotid arteries, that supply the head and neck with oxygenated blood, is responsible for 20 % - 30 % of all strokes. Stroke, or cerebrovascular accident (CVA), is the rapid loss of brain functions due to disturbance in the blood supply to the brain. In Italy, as in many developed countries, stroke is the first cause of disability, the second of dementia and the third of death[16]. Left common carothid artery originates directly from aorta while right common carothid originates from the right subclavia artery. In the neck they both divide into two other vessels called external and internal carotid arteries. The point at which the common carotid divides is very often the place of formation of an atherosclerotic plaque.

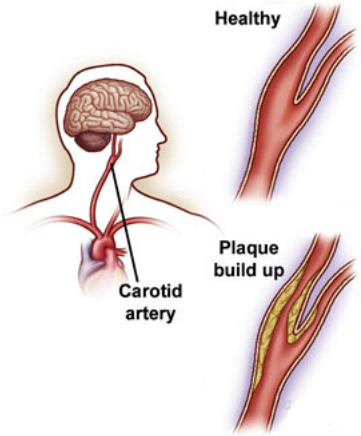

Figure 4.2: **Carotid artery**. We can see carotid artery position and also its conformation

There are many factors that play a role in the development of atherosclerosis. Some of these factors are not depending of lifestyle and include age, race, sex, genetic, diabetes mellitus, hypertension. Other are modifiable and

include smoking, hyperlipidemia, sedentary habits, alcohol and substance abuse. The geometry of the carotid bifurcation itself can be considered a risk factor [2].

Atherosclerosis is a chronic disease. The process that leads to the formation of atherosclerotic plaque can last many years. Most people with carotid stenosis have no symptoms until the artery becomes severely narrowed. As we age, hypertension and small injuries to the blood vessel wall can allow plaque formation. Plaque is a sticky substance made of cholesterol, calcium and other fibrous material. Over time, plaque deposits inside the inner wall of the artery can form a large mass that narrows the lumen (i.e. the inside diameter of the artery). As the atherosclerotic plaque develops, the biologic response is cover the plaque with a fibrous cap. Unfortunately, over time the fibrous cap may rupture and release the underlying debris into the circulation.

Stenosis is not the only effect. Artherosclerotic changes include diffuse intimal thickening that results from the migration of medial smooth muscles cells into the subendothelial space. This fact causes the change of the mechanical characteristic of the artierial structure where a plaque has formed. Some works, as [7] , pointed out a non-elastic behaviour of the atherosclerotic arteries. However consider a more simple model is possible, taking account of the hardening caused by the plaque setting the elastic coefficient of the tissue where the plaque is situated higher than in the rest of the wall [16].

Surgical treatment is generally recommended for patients who have suffered strokes or have a moderate to high grade of carotid stenosis. The operation consist in remove plaque and so enlarge the artery lumen to allow more blood flow to the brain.

In this work we considered a patient that had been subjected to such surgical treatment close to the bifurcation of the left common carotid. MRI images [1] before and after the plaque removal allowed to reconstruct the computational domain of the patient at hand before and after the operation. We considered three configurations:

⇒ The carotid after the operation;

⇒ The carotid before the operation with uniform tissues characteristics;

⇒ The carotid before the operation increasing tissues stiffness where the plaque was.

[1]Magnetic resonance imaging (MRI) also called nuclear magnetic resonance imaging (NMRI), or magnetic resonance tomography (MRT) is a medical imaging technique used in radiology to visualize internal structures of the body

4.2 Setting of the boundary conditions and sensitivity of the numerical solution respect to the mesh

Before doing the simulations we had to set some initial parameters related to the boundary conditions. We will explain later in this section how had been formulated the boundary conditions. We performed simulations of the carotid after surgery with the aim of setting these parameters in order to obtain physiological values of pressure at systole (between 110 and 120 mmHg) and diastole (between 70 and 80 mmHg). Furthermore we made that the value of maximum velocity at systole in the entry section was as close as possible to the available clinical data for the patient examined.

We proceeded in this way: we made two meshes (i.e. a discretization in nodes for the domain), that we call Mesh1 and Mesh2. In both meshes the distance h between nodes was defined as $h = \epsilon\sqrt{r}$ where r is the internal radius of carotid's lumen in cm and ϵ is a parameter at our disposal. In Mesh1 $\epsilon = 0.5$ and in Mesh2 $\epsilon = 0.35$. We ran all the simulations using Mesh1 with $\Delta t = 2 \cdot 10^{-3} s$ and all the simulation using Mesh2 with $\Delta t = 1 \cdot 10^{-3} s$. First we set all the parameters running several simulations with Mesh1. This mesh require less computing power and less time for one simulation, but guarantees in principle less accurate results. Afterwards we ran a simulation with Mesh 2 using the parameters obtained with Mesh1 to verify the goodness of the choice.

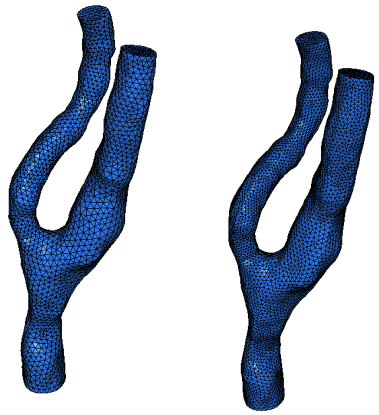

Figure 4.3: Mesh1 and Mesh2 for the fluid domain

1) Robin condition for the surrounding tissue

Vessels are constrained radially by the surrounding tissue. We used a 0D model to describe the presence of a surrounding tissue around the vessel. In particular, we prescribed the following robin boundary condition:

$$\alpha_e \widetilde{\boldsymbol{\eta}}_s + \widetilde{\boldsymbol{T}}_s \widetilde{\mathbf{n}} = P_{ext} \widetilde{\mathbf{n}} \qquad \text{on } \Gamma_{out},$$

where Γ_{out} is the external surface of the vessel and $\widetilde{\mathbf{n}}$ is the normal vector exiting from the structure domain in the reference configuration. We imposed $\alpha_e = 3 \cdot 10^6 dyne/cm^3$.

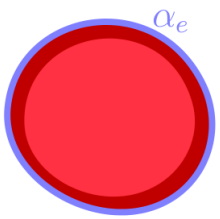

Figure 4.4: **External Tissue**. In blue is evideced the Γ_{out} surface

2) Absorbing boundary condition on the outlet sections

We propose to use a resistance absorbing boundary condition at on the outlet surfaces, that reads:

$$\frac{1}{|\Gamma_{out}|} \int_{\Gamma_{out}} (\boldsymbol{T}_f \mathbf{n}) \cdot \mathbf{n} \, d\sigma + R \int_{\Gamma_{out}} \boldsymbol{u} \cdot \mathbf{n} \, d\sigma = P_{ext}$$

where Γ_{out} are the outlet surfaces and $R = R(P_{ext})$. The value of R has been determined by coupling the 3D model for the part of artery simulated with a 1D model that represent the circulatory system downstream(see [16, 10] for further details). This boundary condition allows us to reduce significantly the spurious pressure wave reflections that typically appear in artificially truncated computational domains. However experience show that is not realistic use the parameter R alone, because in the reality some pressure waves reflection from the rest of the circulatory system exist. So we corrected the parameter R with a coefficient named ξ, so that the absorbing condition is defined by the parameter ξR.

3) Flux on the inlet surface

The flow rate F_{in} is imposed at the entry region at every time instant through the Lagrange multipliers method (see [11, 20]): $F_{in} = kAv_{ec}$, where

$k \in (0,1)$, A is the inlet area in cm^2 and v_{ec}, expressed in cm/s, is a clinical data obtained from an Eco Color Doppler exam . This exam gives us an histogram of the maximum velocity of the red blood cells over small volumes of the lumen(see figure 4.5). We need to introduce the parameter k because the maximum computed velocity is not equal to v_{ec}. We fixed this parameter in order to obtain a value for the maximum velocity at inlet section equal to v_{ec} at systole (73 cm/s).

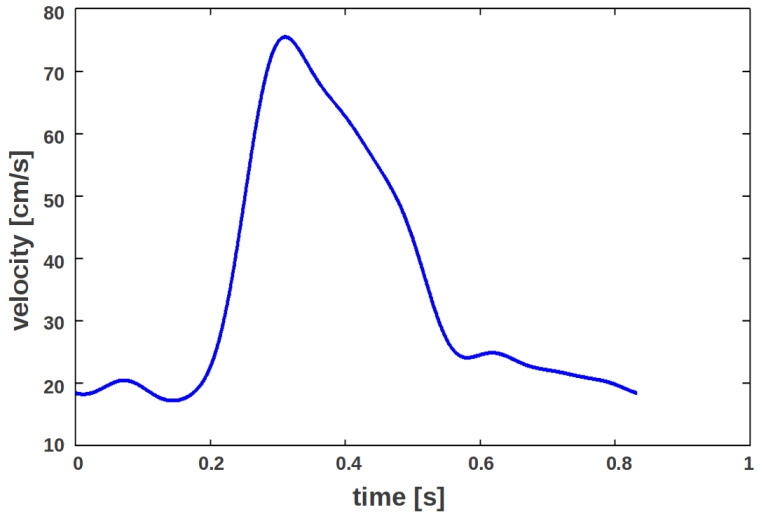

Figure 4.5: The velocity data from Eco Color Doppler

We ran several simulations with Mesh1 until we identified the following set of parameters as the best for the purposes we had: $P_{ext} = 60mmHg$, $k = 0.5$, $\xi = 1.1$. Then we ran a simulation with Mesh2 using the same parameters. The values obtained for pressure are showed in table 4.1.

	Systole	Diastole
Mesh 1	122	76
Mesh 2	121	76

Table 4.1: The values of pressure in mmHg obtained with the two meshes

Moreover we achieved a value of 72 cm/s for the maximum velocity at systole with Mesh1 and 75cm/s for Mesh2.

We can see that there are very little differences between the results obtained with the two meshes. This is a very importan results, because these parameters are specific of the patient. This mean that if we want to take in

exam another patient we can set the parameters running simulations with Mesh1 without the necessity to do a simulation with Mesh2 for validate them. Then we can save time (the simulation of an heartbeat using Mesh1 takes about one week, while with Mesh2 takes one month!) and computing power.

4.3 Comparison before and after the removal of the plaque

We made three simulations to compare the behaviour of the blood flux and of the vessel's wall in presence of an atherosclerotic plaque. In the first we simulated the blood flow in the carotid after the removal of the plaque. In the second we considered the same vessel before the surgical operation of plaque removal but without considering the tissue stiffening caused by atherosclerosis. Finally we ran a simulation in which to simulate the hardening of the tissues in presence of a plaque we set the parameter $\alpha_e = 1 \cdot 10^7 dyne/cm^3$ for the surrounding tissue in the place where the plaque was.

We ran all the simulation using meshes with the parameter $\epsilon = 0,5$. We are conscious that using a smaller ϵ parameter we could get more accurate results but the time at our disposal not allowed us this thing.

For all simulations we impose at the entry section the same velocity data, those obtained after the operation. Indeed our aim was not simulate reality but try to understand how, starting from the same conditions, the change in geometry and vessel's mechanical characteristic can influence blood flow.

The considered patient had a serious atherosclerotic condition at the bifurcation of the left common carothid that results in a reduction of the lumen of about 70 % (see image 4.6). Indeed the lumen area in the considered point was about 0.42 cm^2 after surgery , while before of about 0.15 cm^2. All simulations ran two cardiac cycles but for the results we consider only the second one, because we considered that the first one had less value.

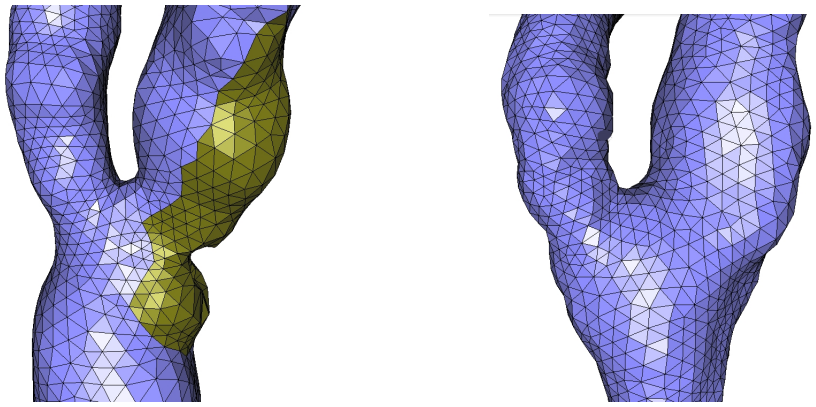

Figure 4.6: The carotid before(left) and after the surgical tratment. Is very evident the reduction in lumen. In yellow we evidenced the plaque

4.3.1 Mean pressure and flux

To value the flux and mean pressure we considered a section just before the bifurcation, that is the place where the plaque was. In the following images we can see the section considered and also the results obtained.

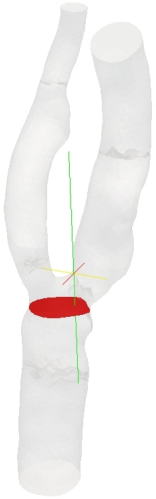

Figure 4.7: The section cosidered for value mean pressure and flux

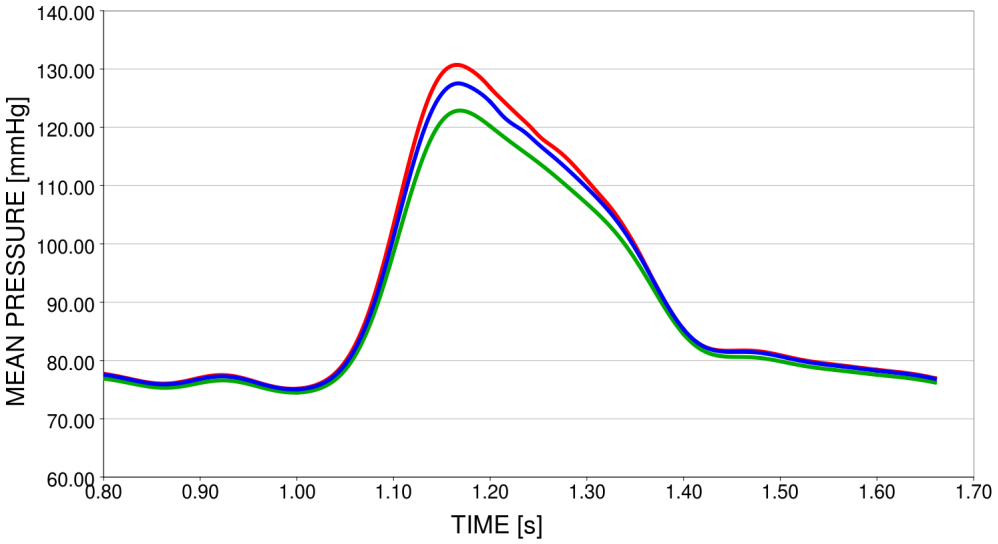

Figure 4.8: The results for the mean pressure during the second heartbeat. In green the result for the carotid after surgical operation. In blue the results for the carotid before the operation and with homogeneous tissue characteristics, in red the results for the carotid before operation with a more rigid tissue near the plaque.

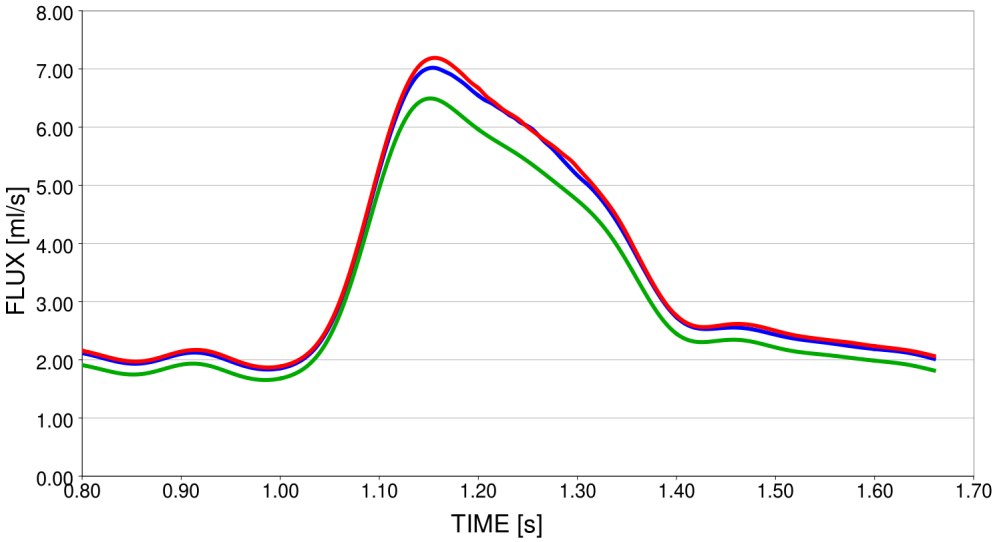

Figure 4.9: The results for the flux during the second heartbeat. In green the result for the carotid after surgical operation. In blue the results for the carotid before the operation and with homogeneous tissue characteristics, in red the results for the carotid before operation with a more rigid tissue near the plaque.

As we can see in figure 4.8 the pressure at systole is significantly higher in the carotid before surgery and this fact agrees with the medical experience,

but it is very important to notice that the gain in pressure is due not only by the tissues hardening but mainly by the stenosis(about sixty percent). In the simulation with only the stenosis the gain in pressure just before the plaque can maybe be explained from the smaller passage area that cause more friction losses: then an higher pressure before the stenosis is "required" to guarantee the imposed flux trough the vessel. In the simulation with tissue hardening the vessel's less elasticity contributes to increase pressure at systole.

Conversely the result for flux are quite different from expected. Indeed in figure 4.9 we can see a small gain in the value of the flux in the carotid before surgery. A decrease in blood flow is usual in atherosclerotic vessels [7]. This not realistic results is maybe due to the fact that we have considered the same inlet data (obtained after the treatment) for all simulations. We remember that our aim was not simulate reality but try to understand how, starting from the same conditions, the change in geometry and vessel's mechanical characteristic can influence blood flow.

4.3.2 Velocity

Now we will consider the results obtained for the velocity field, examining the data obtained at the systole for all three simulations.

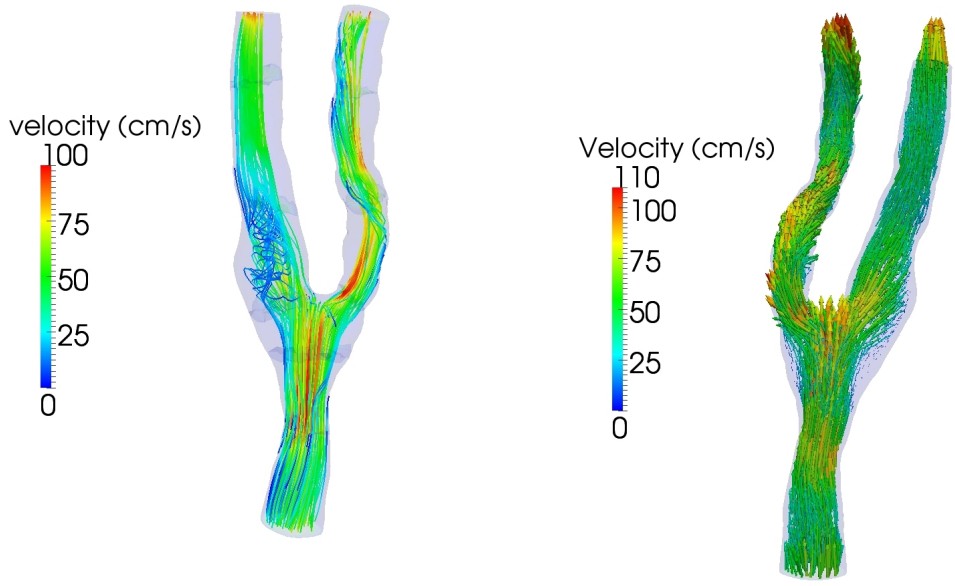

Figure 4.10: The streamlines and the velocity vectors at the systole of the carotid after the surgery

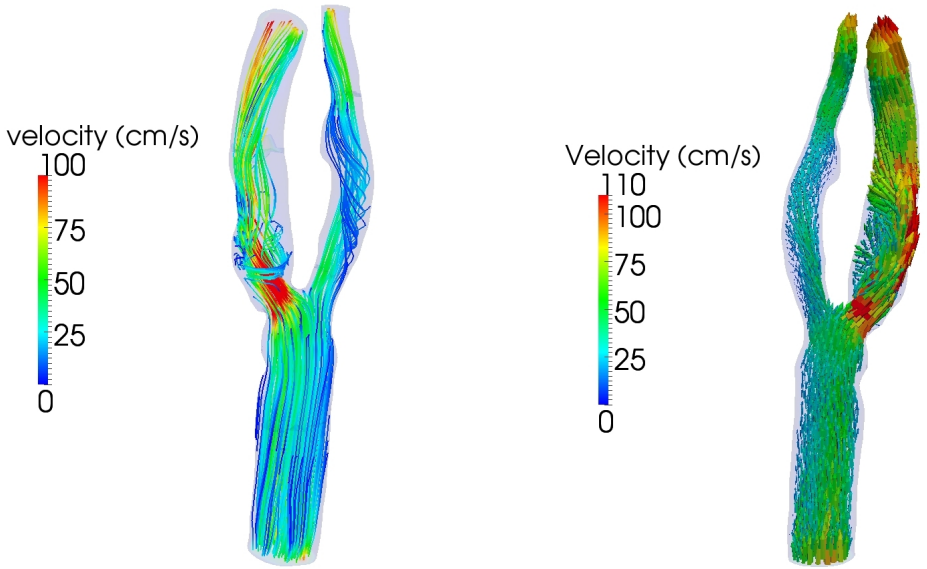

Figure 4.11: The streamlines and the velocity vectors at the systole of the carotid before the surgery not considering tissue hardening

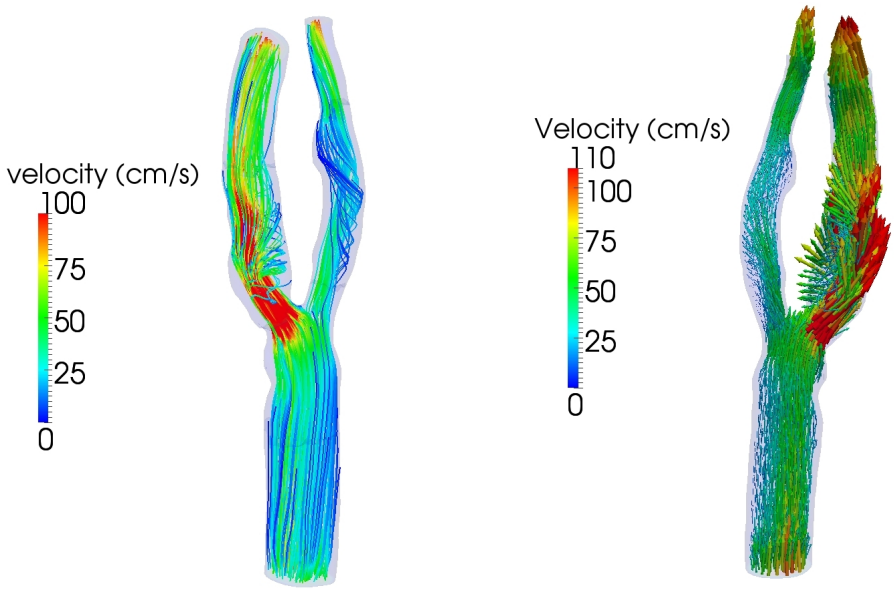

Figure 4.12: The streamlines and the velocity vectors at the systole of the carotid before the surgery considering tissue hardening

It is very clear from the images that before the surgical operation the velocity at the stenosis is higher than after the operation. The effect is greater in the simulation with the tissues hardening, as can be expected

because we have higher values for flux (see figure 4.9) but less lumen area: indeed tissue hardening causes less wall displacement (as it will be showed in next section) and so the lumen vessel becomes less large at systole.

4.3.3 Wall displacement

In the following images we will show the result obtained for the displacement of the vessel wall at the fluid-solid interface.

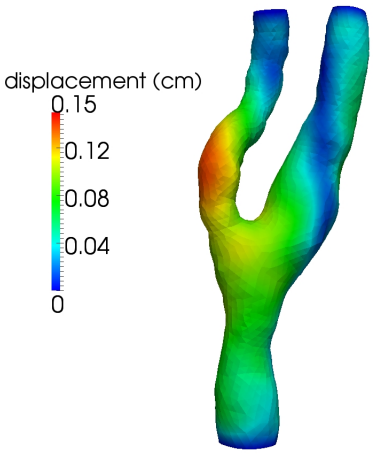

Figure 4.13: The displacement of the wall at the systole of the carotid after the surgery

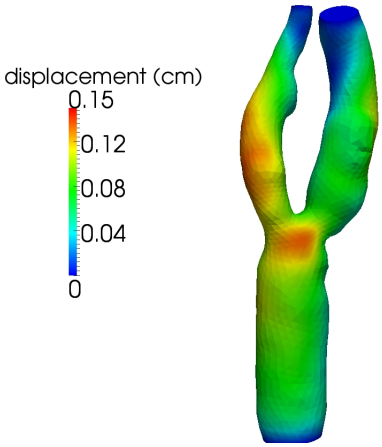

Figure 4.14: The displacement of the wall at the systole of the carotid before the surgery (not considering tissue hardening)

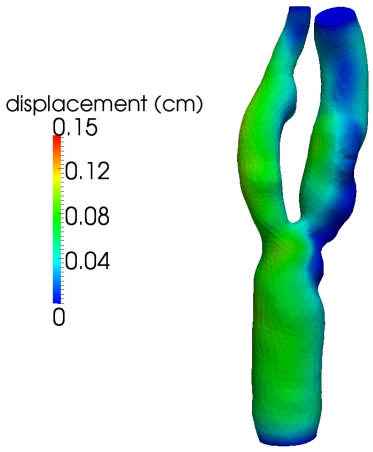

Figure 4.15: The displacement of the wall at the systole of the carotid before the surgery (considering tissue hardening)

As expected the value of wall displacement is lower in the case where the plaque hard tissue has been implemented respect to other two cases. It can be noticed that in the simulation after the surgery and in the simulation before surgery but without tissue hardening the values of displacement are comparable. This mean that, as can be expected, low wall displacement is caused by the tissue stiffening and not by stenosis.

4.3.4 Wall shear stress (WSS)

In next images we can see the results obtained for shear stress at the fluid-structure interface.

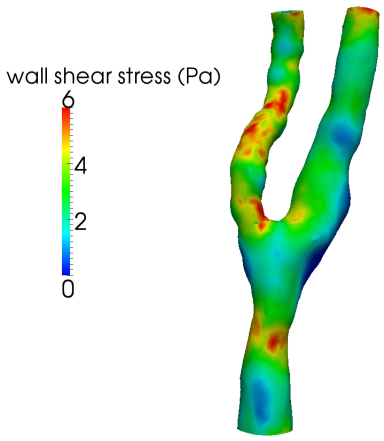

Figure 4.16: The displacement of the wall at the systole of the carotid after the surgery

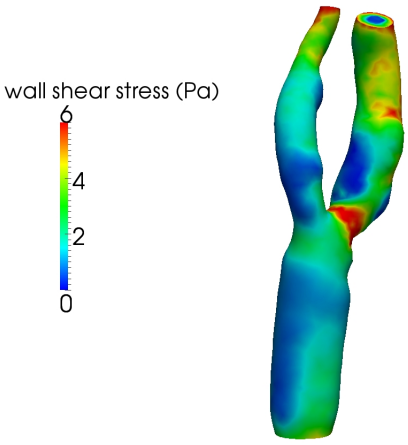

Figure 4.17: The displacement of the wall at the systole of the carotid before the surgery (not considering tissue hardening)

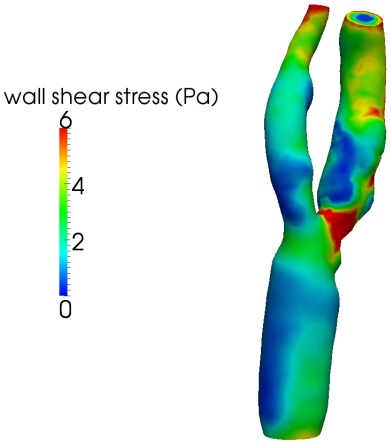

Figure 4.18: The displacement of the wall at the systole of the carotid before the surgery (considering tissue hardening)

Wall shear stress influence the orientation and deformation (or even damaging) of the endothelial cells. Wall permeability, and the possibility to change the chemical composition and mechanical characteristic of the vessel wall therefore depends on wall shear stress [3]. Furthermore has been suggested that an high value of WSS is the cause of the plaque rupture, that is the main danger in this situations, because the particles of the plaque relased in blood flow can obstruct smaller vessels and then cause ischemic attacks [5]. The value of wall shear stress (WSS) is greater near the stenosis in the simulations of the carotid before the surgery but above all in the case where

the tissue stiffening have been considered. Indeed WSS in a Newtonian fluid is is directly proportional to velocity gradient, that is higher in the carotids before the operation, because the value of fluid velocity is itself greater (see section 4.3.2). Velocity gradient is higher in the case where tissue stiffening have been considered, not only because the value of maxium velocity is greater but also because the velocity of the structure is lower, and this made that WSS reached its maximum values in this case.

4.4 Final comment on the results obtained

In the first part of our work we discussed about the setting of the boundary conditions necessary to define the mathematical model that we used to simulate blood flow in human carotids. We obtained an important result: we can set the parameters that define the boundary conditions without increasing too much the accuracy of the mesh. Indeed we showed that using the same paremeter with a more accurate discretization we obtained similar values for the quantities that we have to control for setting the parameters.

Then in the second part we tried to understand how, starting from the same inlet conditions, some important parameters change in a carotid subjected to a surgical treatment of atherosclerotic plaque removal. Most of the results obtained with the simulations agree with the the clincal data and results obtained in other works as [16].

An important result is that in the carotid before the surgery the values of blood pressure, in particular at systole, are higher than in carotid after the treatment. This agree with medical experience, but according to the simulations this gain in pressure is caused not only by the more stiffness of the tissues in presence of the plaque but mainly by the reduction in lumen area (about sixty percent of the gain at systole is due by stenosis). This results can maybe be explained from the smaller passage area that cause more friction losses: then is "required" an higher pressure before the stenosis to guarantee the imposed flux trough the vessel. In the simulation with tissue hardening the vessel's less elasticity contributes to increase pressure at systole.

Another important and expected result is the lower deformation of the carotid's wall together with higher values of wall shear stress. In some works, as in [5], has been suggested that this fact is the cause of the plaque rupture, that is the main danger in this situations, because the particles of the plaque relased in blood flow can obstruct smaller vessels and then cause ischemic attacks. More over the possibility to change the chemical composition and mechanical characteristic of the vessel wall depends on wall shear stress [3].

Other results, as the increase of blood flow do not agree with medical experience, and this fact is caused probably by the fact that we have imposed the same velocity conditions, that obtained after the surgical treatment, also on the model of the diseased carotid, a not realistic assumption, as the fact that we simulated only a small part of the complex cardiovascular system.

Bibliography

[1] Quarteroni A. and Valli A. Domain decomposition methods for partial differential equations. *The Clarendon Press*, 1999.

[2] J. Seong C. Sadasivan M. J. Gounis L. Miskolczi A. K. Wakhloo, B. B. Lieber and J. S. Sandhu. Hemodynamics of carotid artery atherosclerotic disease. Technical report, Vasc Interv Radiol.

[3] Alessandro Veneziani Alfio Quarteroni, Luca Formaggia. The circulatory system: from case studies to mathematical modeling. Technical report, Politecnico di Milano.

[4] Fausto Saleri Alfio Quarteroni. *Calcolo scientifico*. Springer, Milano, 2008.

[5] David Calvet Moustapha Zidi Enrico-Agabiti Rosei Stephane Laurent Anna Paini, Pierre Boutouyrie. Multiaxial mechanical characteristics of carotid plaque: analysis by multiarray echotracking system. *Stroke, journal of the american heart association*, 2007.

[6] Steinman D. Image-based cfd modeling in realistic arterial geometries. *Annals of Biomedical Engineering*, 2002.

[7] Sherif Sultan Niamh Hynes Caitri ´Ona Lally Daniel J. Kelly Eoghan Maher, Arthur Creane. Inelasticity of human carotid atherosclerotic plaque. *Annals of Biomedical Engineering*, September 2011.

[8] C.Vergara F.Nobile. Partitioned algorithms for fluid-structure interaction problems in haemodynamics.

[9] C.Vergara F.Nobile, M.Pozzoli. Time accurate partitioned algorithms for the solution of fluid-structure interaction problems in haemodynamics. part 2: The finite elasticity case. *In preparation.*

[10] C.Vergara F.Nobile, M.Pozzoli. Time accurate partitioned algorithms for the solution of fluid-structure interaction problems in haemodynamics. *International journal for numerical methods in engigneering*, 2012.

[11] Nobile F Quarteroni A Formaggia L, Gerbeau JF. Numerical treatment of defective boundary conditions for the navier-stokes equation. *SIAM Journal on Numerical Analysis*, 2002.

[12] Alfio Quarteroni Alessandro Veneziani Luca Formaggia, Fabio Nobile. Multiscale modelling of the circulatory system: a preliminary analysis. *Computing and Visualization in Science*, June 1999.

[13] Alessandro Veneziani Massimiliano Tuveri, Alfio Quarteroni. Computational vascular fluyd dynamics: problems, models and methods. *Computing and Visualization in Science*, August 1999.

[14] F.Nobile P.Causin, J.F. Gerbeau. Added-mass effect in design of partitioned algorithms for fluid-structure problems. *Computer Methods in applied mechanics and engigneering*, December 2004.

[15] Matteo Pozzoli. Simulazioni numeriche per l'interazione fluido-struttura in emodinamica. Degree thesis, Politecnico di Milano, Mathematical Engineering.

[16] Matteo Pozzoli. Efficient partitioned algorithms for the solution of fluid-structure interaction problems in haemodynamics. Ph.d thesis, Politecnico di Milano, Mathematical Engineering, February 2012.

[17] Francesco Premoli. Emodinamica e aterosclerosi: simulazioni numeriche per problemi di interazione fluido-struttura. Degree thesis, Politecnico di Milano, Aeronautical Engineering, 2009.

[18] Alfio Quarteroni. What mathematics can do for the simulation of blood circulation. Technical report, Politecnico di Milano.

[19] Alfio Quarteroni. *Modellistica numerica per problemi differenziali*. Springer, Milano, 2008.

[20] Vergara C. Veneziani A. Flow rate defective boundary conditions in haemodinamics simulations. *Journal for Numerical Methods in Fluids*, 2005.

[21] Nichols W. and O'Rourke M. *Mc Donald's Blood Flow in Arteries*. Edward Arnold Ltd, London, 1990.